Contents lists available at ScienceDirect

Chemical Physics Letters

Pressure-induced morphology-dependent phase transformations of nanostructured tin dioxide

Zhaohui Dong, Yang Song *

Department of Chemistry, The University of Western Ontario, London, Ontario, Canada N6A 5B7

ARTICLE INFO

ABSTRACT

Two morphologies of nanostructured tin dioxide (SnO_2) (i.e., nanobelts and nanowires) were compressed in diamond anvil cells up to 38 GPa followed by decompression. *In situ* Raman spectroscopy and synchrotron X-ray diffraction were employed to monitor the structural transformations. It was found that nanostructured SnO_2 behaved drastically differently than bulk material in terms of transformation pressures, phase stability regions and compressibility. These findings provide new insight into the unique pressure behaviours of nanostructured materials and have profound implications for producing controlled structures with new applications achieved by combined pressure-morphology tuning.

© 2009 Elsevier B.V. All rights reserved.

1. Introduction

Nanostructured inorganic materials in different morphologies such as dots, wires and belts are of fundamental importance because of their wide range of tunable electrical, optical and mechanical properties. Investigations of the structures and phase transformations of nanomaterials under high pressures have received increasing attention [1–16]. This is simply because, in addition to composition and synthetic routes, high pressure provides an additional effective driving force to produce new structures and, therefore, new nanomaterial properties [13]. The most interesting aspect of high-pressure studies on nanomaterials is the observation that compressed nanomaterials exhibit significantly different behaviours than their corresponding bulk counterparts, such as the size-dependent phase transformations observed for nano-scale CdSe [1,2], SnO_2 [8,11] and TiO_2 [14]. In addition, morphology can play an important tuning role in the pressure-induced transformations of nanostructured materials. For instance, ZnS nanobelts have been found to exhibit a much wider stability region up to 6.8 GPa for the wurtzite phase, in strong contrast to bulk ZnS, which is much more stable in the sphalerite phase [12]. This demonstrates that pressure combined with size and morphology can dramatically alter the structure and stability of nanomaterials.

Here we report novel pressure behaviours for nanostructured tin dioxide (SnO_2). As an *n*-type semiconductor with a large band gap (E_g = 3.6 eV at 300 K), SnO_2 has been studied extensively for applications in transparent conducting electrodes, lithium ion batteries and gas sensors [17]. Specifically, because SnO_2 exhibits high sensitivity for detecting CO and NO_x gases, rigorous studies on SnO_2-based gas sensors have been undertaken [17]. In these stud-

ies, SnO_2 in orthorhombic structures was found to exhibit better sensitivity for specific gases than the tetragonal rutile-type structure [18,19]. However, natural SnO_2, known as cassiterite, always exists as the rutile-type structure and it is generally difficult to obtain the orthorhombic phase directly from minerals [20]. Therefore, finding new methods for producing SnO_2 with orthorhombic structures, such as by pressure tuning [21], is of particular interest in the sensor industry. In addition, studies suggest that nanostructured SnO_2 might exhibit significantly enhanced performance for certain gas-sensing applications than thick films or bulk materials [22]. Therefore, many nanostructured SnO_2 morphologies, including nanoparticles, nanowires, nanorods and nanobelts, have been synthesized [23–25] and their optical and electrochemical properties evaluated. Spectroscopic studies such as Raman measurements [26] and photoluminescence [25] show that SnO_2 nanobelts exhibit unique optical properties that are different than those from bulk materials. These recent studies motivated us to undertake the first the high-pressure investigations on the behaviours of one-dimensional nanostructued SnO_2, resulting in the observation of novel, unexpected nano-effects.

2. Experimental

SnO_2 nanobelts and nanowires were synthesized using chemical vapor deposition on silicon substrate, starting with SnO powders (99%, Alfa Aesar). The experimental details have been described elsewhere [25,27]. The morphologies and chemical composition of SnO_2 nanobelts and nanowires were examined by SEM (Leo/Zesis 1540XB FIB/SEM) and energy dispersive X-ray spectroscopy.

SnO_2 nanobelts and nanowires were removed from the substrate and were loaded into diamond anvil cells (DACs) for subsequent characterization. A symmetric DAC with a pair of type I

---

* Corresponding author. Fax: +1 519 6613022.
  E-mail address: yang.song@uwo.ca (Y. Song).

diamonds and a 400-μm culet was used. A hole with a diameter of 150 μm was drilled on a stainless steel gasket and used as the sample chamber. A few ruby chips were loaded with the sample as the pressure calibrant. The samples were loaded without pressure transmitting medium (PTM) for Raman measurements, whereas silicon oil was used as the PTM for X-ray diffraction measurements.

Raman experiments were carried out using a customized Raman micro-spectroscopy system. A 488 nm line from an Innova Ar$^+$ laser (Coherent Inc.) was used as the excitation source and was focused to less than 5 μm on the sample by an Olympus microscope. The Rayleigh line was removed using a pair of notch filters. The scattered light was dispersed using an imaging spectrograph equipped with a 1800 lines/mm grating, achieving a resolution of 0.1 cm^{-1}. The scattered light was then recorded using an ultrasensitive liquid nitrogen-cooled, back-illuminated CCD detector from Acton. The system was calibrated using neon lines with an uncertainty of ±1 cm^{-1}.

The angle dispersive X-ray diffraction measurements were carried out at the X17C beamline at the National Synchrotron Light Source (NSLS) at Brookhaven National Laboratory (BNL). A high-energy, fixed-exit monochromator with Sagittelly-bent double Si crystal Laue mode was used to optimize the high-energy synchrotron X-ray from 20 keV to 40 keV, with an incident X-ray wavelength of 0.4066 Å. A pair of Kirkpatrick–Baez (KB) mirrors consisting of Si crystals coated with Pt and a focal length of 100 mm were used to focus the white X-ray beam at a glancing angle of approximately 1 mrad. This focused a 180×180 μm incident beam to a 25 μm (horizontal) $\times$ 25 μm (vertical) beam on the sample. A MAR CCD X-ray detector was used to collect the 2D Debye–Scherrer patterns. The gonioemeter geometry and other diffraction parameters were calibrated using CeO$_2$ standard diffraction. Each diffraction pattern was obtained during an average exposure time of 5–10 min. The two-dimensional Debye–Scherrer patterns were converted to one-dimensional diffraction patterns using Fit2D software and Rietveld refinements were performed using Gsas package.

3. Results and discussion

Fig. 1a and c shows the dimensions and morphologies of the as-made SnO$_2$ nanobelts and nanowires. The nanobelts were several tens of nanometers thick, several micrometers long and a few hundred nanometers up to 1 μm wide. The nanowires were 50–60 nm in diameter and several microns long. Raman measurements were performed on SnO$_2$ nanobelts with selected spectra depicted in Fig. 3. SnO$_2$ nanobelts at ambient pressure had a regular rutile-type structure (space group P4$_2$/mnm or D_{4h}^{14}, Z = 2) and, therefore, the irreducible representation predicted the Raman active modes to be A_{1g}, B_{1g}, B_{2g} and E_g, with three bands observed at 473 cm^{-1} (E_g), 631 cm^{-1} (A_{1g}) and 773 cm^{-1} (B_{2g}), consistent with previous Raman measurements on nanostructured SnO$_2$ [26]. Additional weak Raman bands at 500 cm^{-1} and 692 cm^{-1} can be assigned as A_{2u} (TO) and A_{2u} (LO) modes, both of which are IR active, whereas the band at 544 cm^{-1} was a Raman forbidden B_{1u} mode. These abnormal Raman bands are characteristic of SnO$_2$ nanobelts and are not observed in the Raman spectrum of bulk SnO$_2$ [26]. Four additional Raman active modes were observed below 300 cm^{-1} (not shown here), which can be attributed to the impurities of the substoichiometric Sn$_2$O$_3$/Sn$_3$O$_4$ phases in the synthetic process [27]. Interestingly, no strong Raman active modes were observed for the SnO$_2$ nanowires, which is in contrast to a Raman study by Zhou et al. [28] on single crystalline SnO$_2$ wires. It is well known that the optical properties of nanomaterials, especially their Raman features, are very sensitive to a number of factors including size, morphology, synthetic route, purity, as well as short-range structures and environment [29]. As a result, different Raman measure-
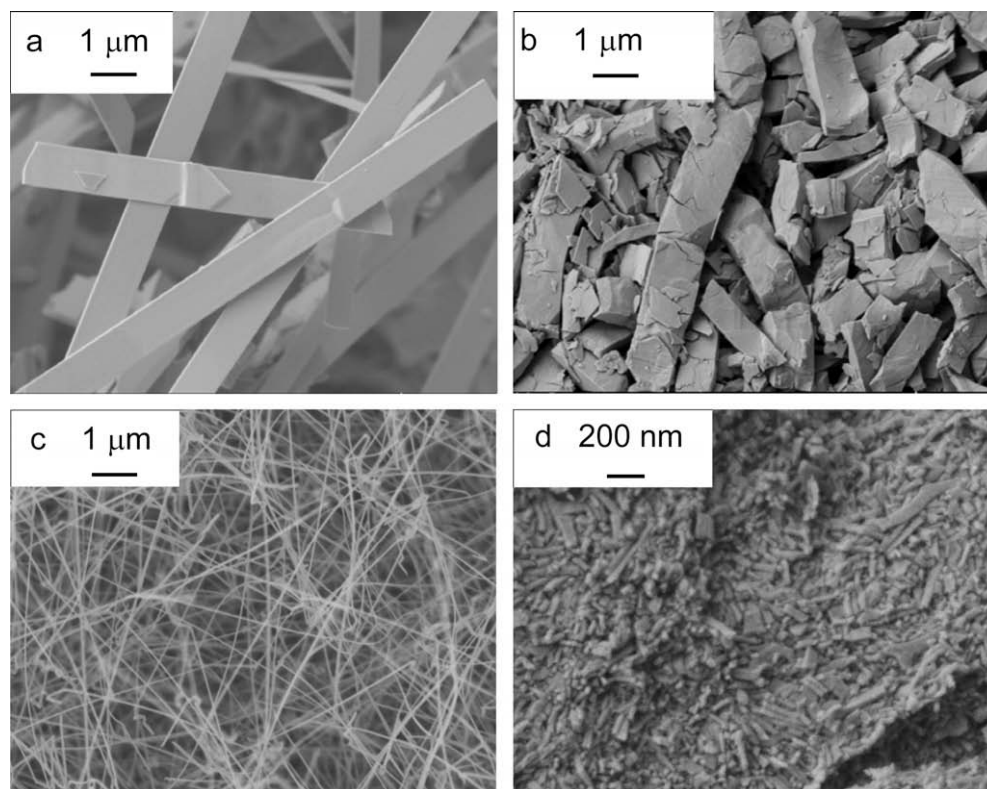

Fig. 1. SEM images of SnO$_2$ nanobelts before compression (a) and after decompression (b) as well as SnO$_2$ nanowires before compression (c) and after decompression (d) with scales shown in each panel.
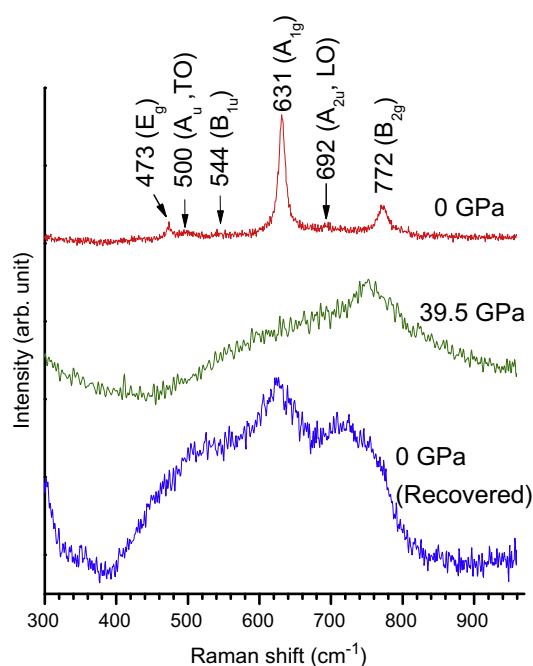
Fig. 2. Raman spectra of SnO$_2$ nanobelts in the spectral region of 300–1000 cm^{-1} collected at ambient pressure (top), at 39.5 GPa (middle) and upon decompression (bottom). The assignments of the observed Raman modes are labeled above the ambient pressure spectrum.
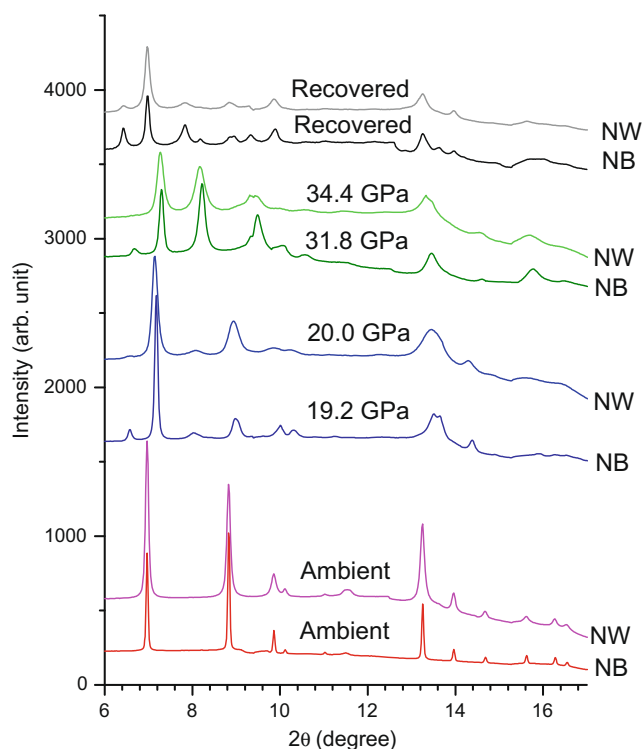

Fig. 3. Representative X-ray diffraction patterns for SnO$_2$ nanobelts (labeled as 'NB' along each pattern) in comparison with SnO$_2$ nanowires (labeled as 'NW' along each pattern) at similar pressures. The pressures or the conditions under which the patterns were obtained are also labeled above each pattern.

ments on the same materials (e.g., various metal oxides) but with different nano-parameters have been reported and analyzed extensively [30,31]. Upon compression, all SnO$_2$ nanobelt Raman modes exhibited a blue shift with decreasing intensities along with profile

broadening. At the highest pressure, only the A_{1g} mode was observed to have a significantly broadened profile (middle spectrum of Fig. 2). Upon decompression, the Raman profiles changed very gradually as the pressure decreased. As the SnO$_2$ nanobelts returned to ambient pressure (lower spectrum of Fig. 2), the E_g and B_{2g} modes were recovered but the bands remained broadened. These observations indicate the partial reversibility of the SnO$_2$ nanobelt optical responses to compression and decompression, which is coincident with the pressure-induced morphology modifications. The SEM images obtained before compression (Fig. 1a), and after decompression (Fig. 1b), suggest that the belts are crushed to shorter sections that are thicker than the original belts before compression. In contrast, the SnO$_2$ nanowires exhibited more dramatic changes in morphology as a result of compression, i.e., the wire shapes were no longer recognizable (Fig. 1d).

In situ high-pressure angle dispersive X-ray diffraction measurements were performed on SnO$_2$ nanobelts and nanowires on compression up to 38 GPa followed by decompression. Representative diffraction patterns are depicted in Fig. 3. Fig. 4 shows the quantitative analysis of the nanobelt diffraction patterns at 31.8 GPa and the nanowire diffraction patterns at 34.4 GPa using
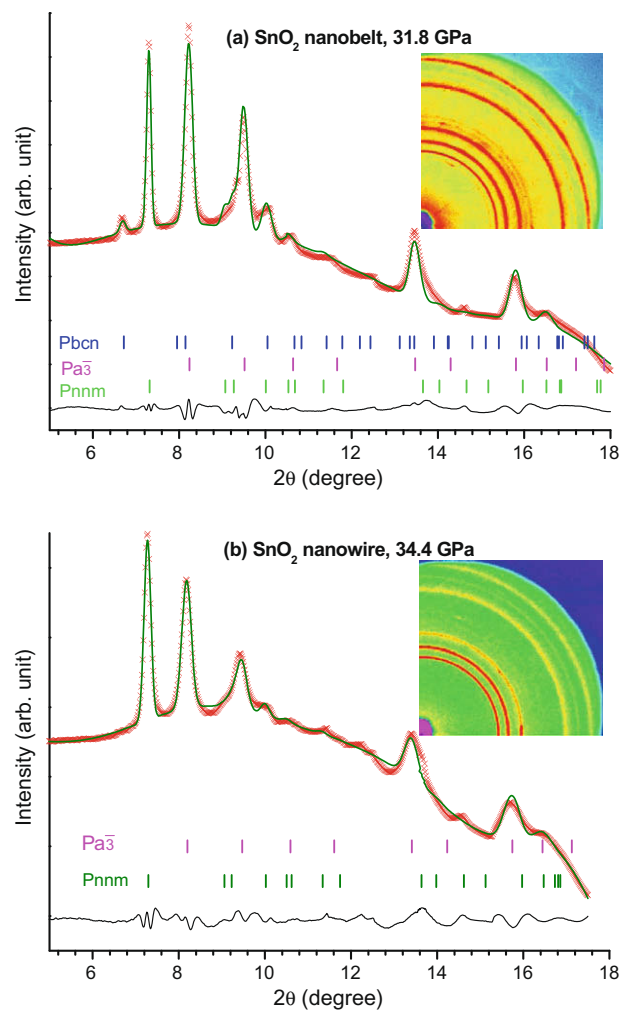

Fig. 4. Rietveld refinement of observed X-ray diffraction patterns for SnO$_2$ nanobelts at 31.8 GPa (a) and for SnO$_2$ nanowires at 34.4 GPa (b), both upon compression. The inset shows the original 2D Debye–Scherrer patterns with one quadrant. The red cross is experimental X-ray intensity whereas the green solid line is the calculated diffraction pattern based on refinement with the black curve at the bottom showing the difference between the calculated and observed intensities. The vertical bars with different colours indicate the characteristic reflections of different phases labeled in the front.

Rietveld refinement. Starting at ambient pressure, the diffraction pattern of SnO_2 nanobelts indicates an excellent crystalline phase that adopts a rutile structure ($P4_2/mnm$) that is the same as that for the bulk material [21], with cell parameters of $a = 4.7218$ Å and $c = 3.1802$ Å. All the diffraction patterns can be indexed with a single rutile-type phase until compressed to near 15 GPa. The broadening of the (1 0 1), (2 0 0) and (2 1 1) reflections of the rutile phase suggests that an orthorhombic phase has formed ($CaCl_2$-type structure with space group *Pnnm*). Rietveld refinement suggests that there was only a slight modification in the cell parameters from the rutile structure: $a = 4.6543$ Å, $b = 4.5744$ Å and $c = 3.1483$ Å. This pressure-induced phase transformation was similar to that observed in bulk SnO_2 [21], but the transformation pressure was higher. SnO_2 nanobelts existed in this single phase up to 19.2 GPa beyond which new phase transformations were observed. The new reflections at 2θ of 6.606° and 8.129° were characteristic of a new orthorhombic α-PbO_2 phase (*Pbcn*) at (1 1 0) and a cubic fluorite phase ($Pa\overline{3}$) at (1 1 1) directions, respectively (Fig. 3). From 19.2 GPa to the highest pressure in the present study, SnO_2 existed as a mixture of these three phases (Fig. 4a). This observation is in strong contrast to the phases observed for bulk SnO_2 materials, in which both the $CaCl_2$-type and α-PbO_2 phases are reported to exist between 12 and 21 GPa [21]. Upon decompression, the three-phase mixture was found to persist down to 7.5 GPa, when the cubic fluorite phase disappeared, with a subsequent back transformation to the rutile structure. Upon complete decompression, the SnO_2 nanobelts were composed of mixtures of rutile and α-PbO_2 phases (Fig. 3). Fig. 5 summarizes these strongly contrasting pressure-induced phase transformations of SnO_2 nanobelts compared with bulk materials.

Upon compression and decompression, SnO_2 nanowires exhibit unexpected pressure responses that are different than those for nanobelts or bulk materials. Starting with the same rutile structure, transformation to a $CaCl_2$-type orthorhombic structure was observed when it was compressed to 17 GPa, which is a higher transition pressure than that for the nanobelts and much higher ($\Delta P > 5$ GPa) than that for the bulk materials. When further compressed to 25 GPa, a fluorite-type phase was found to contribute to the overall diffraction pattern and coexisted with the $CaCl_2$-type phase all the way to the highest pressure. A striking observation that the α-PbO_2 phase was missing in the entire compression region was noted. Fig. 4b shows the Rietveld refinement analysis of the diffraction pattern, which unambiguously suggests that the SnO_2 nanowires are composed of only $CaCl_2$-type and fluorite-type phases at 34.4 GPa. Upon decompression, the $CaCl_2$-type phase transformed back to the rutile-type phase at 16 GPa, which is much earlier than that observed for either nanobelts or bulk materials. Further decompression results in more surprising transformations – the fluorite-type phase persists all the way to near-ambient pressure, whereas the α-PbO_2 phase that was missing during compression was observed when it was decompressed to 10.6 GPa and was recovered at ambient pressure (Fig. 3). These transformations are also summarized in Fig. 5 and compared with those observed for nanobelts and bulk materials.

Rietveld refinement performed on all diffraction patterns indicated that the rutile and $CaCl_2$-type phases were the dominant phases both for nanobelts and nanowires, whereas the α-PbO_2 and flurorite phases contribute to the mixed phases only to a certain extent. Therefore, we fit the third-order Birch equation of state (EOS) based on only the dominant phases of nanobelts and nanowires to estimate the compressibility. The bulk modulus and its first derivative were $B_0 = 169.3$ GPa and $B' = 8.4$ for the nanobelts whereas those for the nanowires were $B_0 = 225.3$ GPa and $B' = 8.1$, respectively. We note that the compressibility of the nanobelts was significantly higher than that for the bulk material ($B_0 = 204$ GPa, $B' = 8.0$) [21], whereas the nanowires were less compressible.

The differences in the pressure-induced phase transitions between nanostructured and bulk SnO_2 materials have been observed for other morphologies, primarily nanoparticles. However, contrasting results were reported by different groups – He et al. found that transition pressure increases with decreasing SnO_2 nanocrystal size [11], whereas Jiang et al. observed no obvious size-dependent transition pressure differences [8]. For other nanostructured materials such as oxides, sulfides or elements, transition pressure shifts have been found to go in both directions. The majority of these nanomaterials (e.g., CdSe [1,2], ZnS [5] and PbS [6]) exhibit higher transition pressures than bulk materials do and their transition pressures also increase with decreasing nanocrystal size [2]. However, other nanocrystal oxides, such as γ-Fe_2O_3 [4] and CeO_2 [32], have reduced transition pressures. The general understanding of the 'size' effect in pressure-induced transformations is to examine a thermodynamic function, i.e., the Gibbs free energy change (ΔG) with the major contributing factors: the ratio of the volume collapse ($P\Delta V$), the surface energy differences ($A\Delta\gamma$) and the internal energy differences (ΔU) [12,33]. It is believed that enhanced transition pressures in nanomaterials indicate that surface energy differences are playing a dominant role, whereas reduced transition pressures might be associated with a compression process overwhelmed by volume collapse. The 'size' effect also seems to extend to one-dimensional nanomaterials such as ZnS nanobelts [12]. Indeed, it was found that the reduced ZnS nanobelt thickness resulted in a higher transition pressure [12]. Therefore, these principles can be adopted to explain some of the pressure-induced transformations observed in this study. The higher transition pressures observed both in nanobelts and nanowires indicates that there is a prominent surface energy effect on nanostructured SnO_2. In particular, the onset pressures involving the rutile-to-$CaCl_2$-type transition are approximately 11.8, 15.0 and 17.0 GPa for bulk materials, nanobelts and nanowires, respectively. Because there is no significant change in the unit cell volume in this transition, the contribution of the first factor, i.e., the ratio of the volume collapse to the overall ΔG, is negligible. Consid-
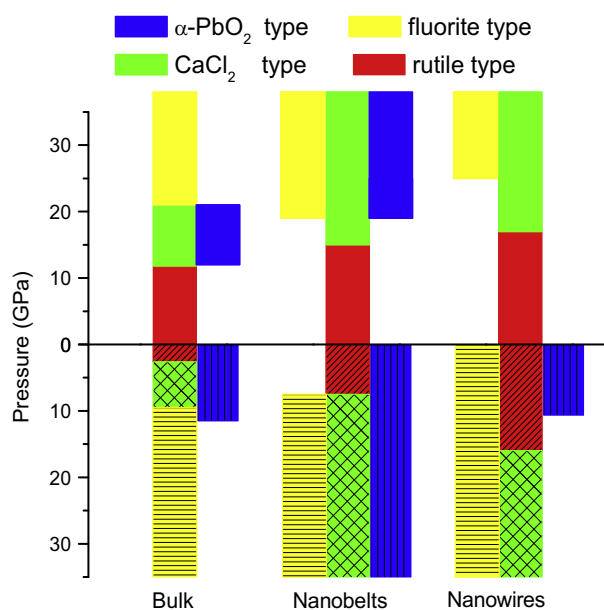

Fig. 5. Summary of pressure-induced phase transformations for SnO_2 nanobelts and nanowires upon compression (plain vertical bars) and decompression (hatched vertical bars) compared with those for bulk SnO_2 material. The different colours label different phases: rutile (red), $CaCl_2$-type (green), flurorite type (yellow) and α-PbO_2 type (blue).

ering that the internal energy differences (ΔU) are typically small or negative [33], the surface energy differences are therefore believed to be mainly responsible for the enhanced transition pressures for nanostructured SnO_2. Gauging from the observed transition pressures, the surface energy differences in the nanowires were estimated to be 62.5% higher than in the nanobelts. Qualitatively, the significantly enhanced nanowire transition pressures can be interpreted by further 'reduced size' from nanobelts with reduced width and thickness. Indeed, the bandwidths of the nanowire reflections are slightly larger in the nanobelts in general (Fig. 3), consistent with the size-induced broadening observed for other nanomaterials [34].

In addition to size effects, morphology has also proven to be an important factor for regulating nanomaterial structure and stability, either by early or delayed phase transitions [12]. However, the drastically contrasting phase stability regions observed for different morphologies of SnO_2, especially for the completely missing α-PbO_2 phase, are unprecedented. On the basis of the above principles, one may speculate that the α-PbO_2 transition pressure might be significantly elevated (i.e., $\gg 38$ GPa), which requires further experimental and theoretical justification. However, such huge pressure increases may well induce other new SnO_2 phases to form [35]. Therefore, the α-PbO_2 phase is likely a metastable phase that cannot simply be interpreted by thermodynamic principles alone. Furthermore, the observed prominent hysteresis, which was characterized by significantly different forward and backward transition pressures, is likely a consequence of different transformation barriers. While the stabilities of difference phases are only determined by thermodynamic functions, the actual transformation pressure may be predominantly governed by kinetics, which scales with the width of the hysteresis. It would therefore be interesting to investigate hysteresis and kinetics as a function of temperature. Indeed, the hysteresis for the nanocrystal CdSe transitions was found to narrow as temperature increased [3]. The combination of pressure, size, morphology, thermodynamics and kinetics has led to the formation of a multi-dimensional structure–property domain with extremely broad tunabilities. Our findings indicate that certain structures and/or phases can be switched 'on' or 'off' at selected pressure regions with selected morphologies via selected paths. Applying pressure to nanomaterials with different morphologies, therefore, has profound implications for producing controlled structures with desirable properties, such as those for gas sensors whose sensitivity has a preferential correlation to the orthorhombic α-PbO_2-type structure of SnO_2 [18]. However, detailed transformation mechanisms, especially the origins of the surprising reversibility and metastability require further theoretical investigation.

Finally, size- and morphology-induced alteration of SnO_2 nanomaterial compressibility characterized by bulk moduli can be understood in parallel with other nanomaterials. CeO_2 nanoparticles exhibit a prominent enhancement of the bulk modulus compared with that for bulk materials [9,34], whereas no obvious difference in compressibility was observed for ZnS nanocrystals [5]. In contrast, the compressibility of PbS and γ-Al_2O_3 [10] was found to increase with decreasing nanoparticle size. Furthermore, strongly contrasting compressibility was observed for TiO_2 nanoparticles, i.e., the bulk modulus of the rice-shaped particles was reduced whereas that of the rod-shaped particles was enhanced by more than 50% relative to that of the bulk materials [16]. Therefore, multiple factors determine the mechanical properties of nanomaterials. In this case, by carefully examining SnO_2 nanobelts at ambient pressure using SEM and Raman imaging [27], other tin oxides (SnO_x) are attached to the nanobelt surface, which could contribute to the defect in the SnO_2 crystal lattice and may therefore decrease the material stiffness. Compared with nanobelts, SnO_2 nanowires carry much fewer or no defects and are more strictly one-dimen-

sional in morphology, which may correlate with their general size-dependent compressibility [9]. These arguments are corroborated by a previous comparative study of nanobelts and nanowires [23].

4. Conclusions

In summary, we have investigated pressure-induced structural evolutions in nanostructured SnO_2 in the form of nanobelts and nanowires in diamond anvil cells using Raman spectroscopy, angle dispersive X-ray diffraction and SEM. We found that nanostructured SnO_2 exhibits drastically contrasting high-pressure behaviours compared with bulk materials, which suggests that nanostructured SnO_2 has significantly different optical, chemical and mechanical properties. These morphology-induced differences for some of the phase transformations can be explained by surface energy differences as the dominant thermodynamics factor, while other phases are primarily mediated by kinetics. These principles may serve as a general guideline for producing novel functional materials with desired stability and/or metastability that may yield promising industrial applications, particularly for semiconductor and chemical sensor uses.

References

[1] S.H. Tolbert, A.P. Alivisatos, Science 265 (1994) 373.
[2] S.H. Tolbert, A.P. Alivisatos, Annu. Rev. Phys. Chem. 46 (1995) 595.
[3] C.-C. Chen, A.B. Herhold, Science 276 (1997) 398.
[4] J.Z. Jiang, J.S. Olsen, L. Gerward, S. Morup, Europhys. Lett. 44 (1998) 620.
[5] J.Z. Jiang, L. Gerward, D. Frost, R. Secco, J. Peyronneau, J.S. Olsen, J. Appl. Phys. 86 (1999) 6608.
[6] J.Z. Jiang, L. Gerward, J. Appl. Phys. 87 (2000) 2658.
[7] K. Jacobs, D. Zaziski, E.C. Scher, A.B. Herhold, P.A. Alivisatos, Science 293 (2001) 1803.
[8] J.Z. Jiang, L. Gerward, J.S. Olsen, Scripta Mater. 44 (2001) 1983.
[9] Z. Wang, S.K. Saxena, V. Pischedda, H.P. Liermann, C.S. Zha, Phys. Rev. B 64 (2001) 012102.
[10] B. Chen, D. Penwell, L.R. Benedetti, R. Jeanloz, M.B. Kruger, Phys. Rev. B 66 (2002) 144101.
[11] Y. He et al., Phys. Rev. B 72 (2005) 212102.
[12] Z. Wang et al., Nat. Mater. 4 (2005) 922.
[13] A. San-Miguel, Chem. Soc. Rev. 35 (2006) 876.
[14] V. Swamy, A. Kuznetsov, L.S. Dubrovinsky, P.F. McMillan, V.B. Prakapenka, G. Shen, B.C. Muddle, Phys. Rev. Lett. 96 (2006) 135702.
[15] Q.X. Guo, Y.S. Zhao, W.L. Mao, Z.W. Wang, Y.J. Xiong, Y.N. Xia, Nano Lett. 8 (2008) 972.
[16] S.-W. Park, J.-t. Jang, J. Cheon, H.-H. Lee, D.R. Lee, Y. Lee, J. Phys. Chem. C 112 (2008) 9627.
[17] J. Watson, K. Ihokura, G.S.V. Coles, Measur. Sci. Technol. 4 (1993) 711.
[18] J. Arbiol, E. Comini, G. Faglia, G. Sberveglieri, J.R. Morante, J. Cryst. Growth 310 (2008) 253.
[19] L. Sangaletti, L.E. Depero, A. Dieguez, G. Marca, J.R. Morante, A. Romano-Rodriguez, G. Sberveglieri, Sens. Actuators, B 44 (1997) 268.
[20] Z. Chen, J.K.L. Lai, C.-H. Shek, Appl. Phys. Lett. 89 (2006) 231902.
[21] J. Haines, J.M. Leger, Phys. Rev. B 55 (1997) 11144.

[22] B. Wang, L.F. Zhu, Y.H. Yang, N.S. Xu, G.W. Yang, J. Phys. Chem. C 112 (2008) 6643.

[23] D. Calestani, M. Zha, A. Zappettini, L. Lazzarini, G. Salviati, L. Zanotti, G. Sberveglieri, Mater. Sci. Eng., C 25 (2005) 625.

[24] D. Calestani, L. Lazzarini, G. Salviati, M. Zha, Cryst. Res. Technol. 40 (2005) 937.

[25] X.T. Zhou, F. Heigl, M.W. Murphy, T.K. Sham, T. Regier, I. Coulthard, R.I.R. Blyth, Appl. Phys. Lett. 89 (2006) 213109.

[26] S.H. Sun, G.W. Meng, G.X. Zhang, T. Gao, B.Y. Geng, L.D. Zhang, J. Zuo, Chem. Phys. Lett. 376 (2003) 103.

[27] F. Wang, X. Zhou, J. Zhou, T.-K. Sham, Z. Ding, J. Phys. Chem. C 111 (2007) 18839.

[28] J.X. Zhou, M.S. Zhang, J.M. Hong, Z. Yin, Solid State Commun. 138 (2006) 242.

[29] G. Gouadec, P. Colomban, Prog. Cryst. Growth Charact. Mater. 53 (2007) 1.

[30] A.K. Arora, M. Rajalakshmi, T.R. Ravindran, V. Sivasubramanian, J. Raman Spectrosc. 38 (2007) 604.

[31] G. Gouadec, P. Colomban, J. Raman Spectrosc. 38 (2007) 598.

[32] S. Rekhi, S.K. Saxena, P. Lazor, J. Appl. Phys. 89 (2001) 2968.

[33] J.Z. Jiang, J. Mater. Sci. 39 (2004) 5103.

[34] Z.W. Wang, Y.S. Zhao, D. Schiferl, C.S. Zha, R.T. Downs, Appl. Phys. Lett. 85 (2004) 124.

[35] S.R. Shieh, A. Kubo, T.S. Duffy, V.B. Prakapenka, G. Shen, Phys. Rev. B 73 (2006) 014105.